Advanced bredigite-containing magnesium-matrix composites for biodegradable bone implant applications

Dezfuli, Sina Naddaf; Huan, Zhiguang; Mol, Arjan; Leeflang, Sander; Chang, Jiang; Zhou, Jie

DOI
10.1016/j.msec.2017.05.021

Publication date
2017

Document Version
Accepted author manuscript

Published in
Materials Science and Engineering C: Materials for Biological Applications

Link to formal publication Materials Science and Engineering: C (Elsevier): https://doi.org/10.1016/j.msec.2017.05.021

Advanced bredigite-containing magnesium-matrix composites for biodegradable bone implant applications

Sina Naddaf Dezfuli[a], Zhiguang Huan[b,*], Arjan Mol[c], Sander Leeflang[a], Jiang Chang[b] and Jie Zhou[a,*]

[a] Department of Biomechanical Engineering, Delft University of Technology, Delft, 2628 CD, The Netherlands
[b] Biomaterials and Tissue Engineering Research Center, Shanghai Institute of Ceramics, Chinese Academy of Sciences, Shanghai, 200050, China
[c] Department of Materials Science and Engineering, Delft University of Technology, Delft, 2628 CD, The Netherlands
*Corresponding authors. Tel: +31 15 278 5357 (Jie Zhou); +86 21 5241 2806 (Z. Huan); E-mail addresses: j.zhou@tudelft.nl (J. Zhou); huanzhiguang@mail.sic.ac.cn (Z. Huan)

ABSTRACT

The present research was aimed at developing magnesium-matrix composites that could allow effective control over their physiochemical and mechanical responses when in contact with physiological solutions. A biodegradable, bioactive ceramic - bredigite was chosen as the reinforcing phase in the composites, based on the hypothesis that the silicon- and magnesium-containing ceramic could protect magnesium from fast corrosion and at the same time stimulate cell proliferation. Methods to prepare composites with integrated microstructures - a prerequisite to achieve controlled biodegradation were developed. A systematic experimental approach was taken in order to elucidate the *in vitro* biodegradation mechanisms and kinetics of the composites. It was found that the composites with 20-40% homogenously dispersed bredigite particles, prepared from powders, could indeed significantly decrease the degradation rate of magnesium by up to 24 times. Slow degradation of the composites resulted in the retention of the mechanical integrity of the composites within the strength range of cortical bone after 12 days of immersion in a cell culture medium. Cell attachment, cytotoxicity and bioactivity tests confirmed the stimulatory effects of bredigite embedded in the composites on the attachment, viability and differentiation of bone marrow stromal cells. Thus, the multiple benefits of adding

bredigite to magnesium in enhancing degradation behavior, mechanical properties, biocompatibility and bioactivity were obtained. The results from this research showed the excellent potential of the bredigite-containing composites for bone implant applications, thus warranting further *in vitro* and *in vivo* research.

Keywords: Magnesium; Bredigite; Composites; Degradation; Mechanical Properties; Bioactivity

1. Introduction

Over the last decade, magnesium has attracted much attention in the field of biomaterials on account of its biodegradable nature and high strength-to-density ratio. In addition, magnesium in its ionic form (Mg^{2+}) is the most abundant bivalent cation within the cells and the fourth most abundant element in vertebrates [1]. Around 64% of the total Mg^{2+} can be found in bone, 35% in other tissue compartments and 1 – 2% in plasma and extracellular fluids [2]. Because of the good biocompatibility and mechanical compatibility of magnesium to human bone, extensive research has been performed to explore the possibilities of using magnesium-based materials for orthopedic implants [3-5]. However, up till now, clinical applications of magnesium-based implants have been rather scarce. Too fast degradation of magnesium-based materials in physiological solutions containing inorganic salts [6], leading to rapid release of hydrogen gas, premature loss of mechanical properties and implant failure, has remained to be a fundamental problem hindering their widespread applications.

Many research efforts have been made to reduce the degradation rate of magnesium by alloying. Although much progress has been made, almost all second phases formed as a result of exceeding solubility limits in the magnesium solid solution have been reported to promote micro-galvanic corrosion, causing localized anodic dissolution of the adjacent magnesium matrix [7]. Consequentially, most magnesium alloys exhibit corrosion rates even greater than pure

magnesium [8]. In addition, constraints have been encountered in using alloying elements, because of known or uncertain long-term clinical effects of these elements. Aluminum, a commonly used alloying element to enhance the strength and corrosion resistance of magnesium, for example, has been reported to cause neurological disorder [9], when its concentration in plasma exceeds 3 μM [10]. Zirconium, an element in the ZK magnesium alloy family, has been found to be associated with liver cancer, lung cancer, breast cancer and nasopharyngeal cancer, when its presence in plasma exceeds 1 mM [11]. Undesirable effects of alloying elements as such have largely limited the adoption of the alloying approach. Surface coating to form a biodegradable layer has been tried as a useful approach to delaying the onset of the biodegradation of the magnesium substrate by preventing the corrosive liquid from reaching the substrate. Obviously, the functionality of the surface coating is limited only to the early stages of immersion in physiological solutions [12], but not during the whole course of degradation, because only the exposed surfaces of an implant can be treated while the bulk remains untreated. Moreover, most biodegradable coatings tend to flake off, once a coated implant is under mechanical loading, which results in localized corrosion of the substrate at an accelerated rate.

Ideally, a biodegradable orthopedic implant is also bioactive and can preserve its functionality over the whole healing period of defected bone (ideally 3 - 6 months) [13]. Magnesium matrix composites containing biodegradable and bioactive particles embedded in the bulk may be able to expose these particles, form a protective layer and stimulate appetite formation throughout the whole course of biodegradation. However, despite the promising potential of magnesium matrix composites for orthopedic applications, up till now, there have been only a few investigations on the subject.

Attempts have been made to use hydroxyapatite (HA) [14, 15] and ß-tricalcium phosphate (ß-TCP) [16, 17] as the reinforcing phases to slow down the degradation of magnesium alloys and improve their bioactivity, mainly considering the close chemical similarities of these bioceramics with the inorganic component of bone. It is the authors' point of view that the choices of these bioceramics were not firmly based on comprehensive considerations to fulfill the requirements of the bioceramic phase in magnesium matrix composites, including biocompatibility, biodegradability, bioactivity, mechanical properties and bondability with the magnesium matrix. As a result, the chosen bioceramics have one or more deficiencies. For example, HA lacks biodegradability, as clinical tests have shown that it does not degrade significantly in the body and remains as a permanent fixture, being susceptible to long-term failure [18]. ß-TCP on the other hand is bioresorbable, but its bioactivity leaves much to be desired, mainly because it lacks silicon that is directly involved in the mineralization process of bone growth [19]. Thus, the incorporation of silicon into Ca-P bioceramics is considered a must, if enhanced bioactivity is desired [20, 21].

Bredigite ($Ca_7MgSi_4O_{16}$) is a biodegradable and bioactive ceramic in the CaO-SiO_2-MgO system. This silicon-containing bioceramic has shown rapid HA mineralization, excellent cytocompatibility [22], a strong stimulating effect on osteoblast proliferation [23] and high osteogenic potential [24]. The mechanical properties of bredigite are close to those of cortical bone [23, 25], enabling bredigite to bear mechanical load over a sustained period of time after implantation, which makes bredigite a more suitable option than the previously used calcium-phosphate-based compounds such as tricalcium phosphates (TCP). One unique property of bredigite lies in its ability to form chemical bonding with the magnesium matrix through a highly exothermic reaction between Si-O bonds of bredigite and magnesium [26], thereby producing MgO and Mg_2Si at the Mg-bredigite interface. It is this property that differentiates the composites with the bioceramics in the CaO-SiO_2-MgO system from the other magnesium-

matrix composites that have so far been studied potentially for orthopedic applications and shown a lack of proper bonding between composite constituents [27]. In other words, bredigite was considered a better choice than HA or TCP in meeting the five requirements of an ideal bioceramic phase for biodegradable magnesium-matrix composites.

In this study, we aimed at developing magnesium matrix composites containing homogenously dispersed bredigite particles and having integrated microstructures in order to (i) slow down the degradation of magnesium, (ii) to extend the duration of its mechanical functionality and (iii) to enhance its bioactivity at the same time. Particular attention was paid to understanding the role that silicon-containing bredigite played in biodegradation and bioactivity mechanisms.

2. Methods

2.1. Material preparation

In this research, a powder metallurgy route was chosen to prepare monolithic magnesium and composite specimens. Magnesium (with a purity of 99.86%, 320 ppm Fe and 160 ppm Ni, determined by means of an X-ray Fluorescence Spectroscope - XRF) and bredigite ($Ca_7MgSi_4O_{16}$) powders with median particle sizes of 90 µm and 10 µm, respectively, were chosen as the starting materials. Irregular bredigite powder particles were mixed with spherical magnesium powder particles at 20 and 40 vol.% using a rotary mixer for 12 h to obtain homogenous mixtures. Subsequently, the mixed powders with 20 and 40 vol. % bredigite particles were heated in a cylindrical die to 350 °C under a pre-pressure of 100 MPa and then compacted at 500 MPa. A sintering step for 2 h under the compaction load was taken to ensure bonding between powder particles.

The value of bulk density (P) was derived from the measured weight and volume of each sample by using Archimedes' principle according to ASTM B962-15.

The microstructures and surface morphologies of the materials were characterized using a JEOL JSM-6500F Scanning Electron Microscope (SEM) working at an accelerating voltage of 15 kV and equipped with an Energy Dispersive Spectrometer (EDS). EDS elemental mapping was conducted to study the elemental compositions of sample surfaces before and after the immersion tests as described below.

2.2. Mechanical properties

Microhardness (Vickers hardness) values of the materials were obtained by micro-indentation with a square-based pyramidal-shaped diamond indenter having an angle of 136° and with a dwelling time of 12 s, according to the standard test method (ASTM E384-99). Samples were indented at 1 kgf. Indentation was repeated at a minimum of 15 times to ensure a reliable mean value. The bulk mechanical properties of the materials were determined by performing compression tests at a crosshead speed of 0.5 mm/min. Compression tests were stopped when the compressive load dropped by more than 20%. The height to diameter ratio of the samples was one, according to ASTM E9. Composite samples were subjected to compression tests before and after immersion in the Dulbecco's modified Eagle's medium (DMEM) solution for 1, 3, 6, 12 days.

2.3. *In vitro* degradation tests

To mimic the situations *in vivo*, degradation tests were conducted in a corrosion cell operating at 37 °C using DMEM (D1145, Sigma-Aldrich) as a corrosive environment. HEPES (4-(2-hydroxyethyl)-1-piperazineethanesulfonic acid - 391338, Calbiochem) - an atmosphere-independent biological buffer was added to DMEM (25 mM) to maintain a certain degree of

electrolyte alkalinity during the degradation tests. An anti-bacterial and anti-fungus agent (A5955, Sigma-Aldrich) was added to DMEM by 1% to prevent bacterial and fungi growth. The ratio of solution volume to sample surface area (SV/SA) was 30 ml/cm^2, according to ASTM G31-72. Before the immersion tests, the exposing surfaces of magnesium and composite samples were ground using SiC sandpaper up to 2400 grit, washed in an ultrasonic ethanol bath for 5 min and dried by a hot air blower. The degradation rates of the materials were determined from the amounts of hydrogen gas released and mass losses. The concentrations of ionic corrosion products in the immersion solution were measured by the Inductive Coupled Plasma (ICP) technique. The changes of the pH of the corrosive solution during immersion were monitored using a micro pH meter (S220 SevenCompact, Mettler Toledo). After the immersion tests, the corrosion products were removed from the samples by using a chromic acid solution composed of CrO_3 (200 g/l) and $AgNO_3$ (10 g/l), according to ASTM G1-90.

2.4. Electrochemical tests

Specimens with a diameter of 13 mm were cut into slices and mounted in epoxy resin with only the top surface to be exposed to the electrolyte, followed by grinding with SiC sandpaper to 2400 grit. The exposed surface area was 1.33 cm^2. The slices were then made conductive by a copper wire with an isolation layer (also shielding the connection area). The three electrode configuration according to ASTM G 5-94 was adopted to perform polarization tests. A Saturated Calomel Electrode (SCE) was used as the reference electrode and a platinum mesh as the counter electrode. Open Circuit Potential (OCP) measurements during immersion up to 24 h were determined using a Solartron 1250/1255 potentiostat. Potentiodynamic Polarization (PDP) tests were performed immediately after the OCP measurements at an initial potential of -0.2 V versus OCP increasing to +0.5 V versus OCP at a scan rate of 1 mV/s.

2.5. In vitro responses of rat bone marrow stromal cells

2.5.1. Cell attachment assay

Rat bone marrow stromal cells (rBMSCs) were used to assess cell attachment to the materials. In brief, cells were resuspended in the cell culture medium and then seeded on to the surfaces of pure Mg and Mg-20% bredigite composite samples with a seeding density of 2 X 10^4 cells per well in 24-well tissue culture plates. After an incubation period of 6 h, specimens were collected from the cell culture plates and rinsed with phosphate-buffered saline (PBS), which allowed the removal of non-adherent cells. The adherent cells were then fixed using 4% paraformaldehyde solution for 30 min. Subsequently, the specimens were treated with 0.1% Triton X-100 in PBS and blocked with 1% bovine serum albumin (BSA) for 20 min. The actin cytoskeletons of the cells were labelled in red by incubating with Phalloidin TRITC (Sigma, USA) for 30 min and in contrast the cell nuclei were labelled in blue by 40,6-diamidino-2-phenylindole dihydrochloride (DAPI, Sigma, USA) [28]. The cell morphology was then observed by using a confocal laser scanning microscope (CLSM, Leica, Germany).

2.5.2. Cytotoxicity tests

Monolithic and composite extracts were prepared with a method established in previous studies [27]. Briefly, magnesium and Mg-40% bredigite discs with a diameter of 13 mm and a thickness of 2 mm were soaked in Dulbecco's Modified Engle's Medium (DMEM, GIBCO) with a surface area to volume ratio of 1 ml/cm^2 and incubated in a humidified incubator at 37 °C and 5% CO_2 for 24 h. The supernatant fluid was withdrawn and centrifuged at 1200 × g for 5 min at room temperature. To obtain desired concentrations of the extracts, the extracts were diluted with DMEM + 10% FBS (Fetal Bovine Serum) (HyClone) + 1% P/S (penicillin/streptomycin) at ratios of 1/2, 1/4, 1/8 and 1/16, and they were then sterilized through a filter (Millipore, 0.22 m) and stored at 4 °C (ISO10993-1).

rBMSCs were adopted to evaluate the cytotoxicity of the materials. Cells were isolated, expanded using an established method with minimum modifications [29] and cultured in DMEM, 10% fetal bovine serum (FBS), 100 U/ml penicillin and 100 mg/ml streptomycin at 37 °C in a humidified atmosphere of 5% CO_2. Cytotoxicity tests were carried out by indirect contact and the control groups involved the use of DMEM as the negative control. Cells were incubated in 96-well cell culture plates at 2 x 10^3 cells/100 µl medium in each well and incubated for 24 h to allow attachment. The medium was then replaced with 100 µl of extracts prepared as aforementioned. The number of viable cells was quantitatively assessed by the MTT test [31]. MTT (Sigma) [3-(4,5-dimethylthiazol-2-yl)-2,5- diphenyl tetrazolium bromide] is a yellow tetrazolium salt that can be enzymatically converted by a living cell to a purple formazan product. The intensity of the color produced is therefore directly proportional to the number of viable cells in culture and thus to their proliferation *in vitro*. The absorbance of the color can be measured at 590 nm (A590). In the present tests, after incubating at 37 °C and in an atmosphere with 5% CO_2 for 1, 3 and 6 days, 100 µl of the 0.5 mg/ml MTT solution was added to the well plate and incubated at 37 $^{\circ}$C for 4 h. Then, 100 µl of dimethyl sulfoxide was added to each well and the plate was shaken for 5 min. The optical density (OD) at 590 nm was measured with an enzyme-linked immunoadsorbent assay plate reader (ELX800, Bio-TEK). The results were compared in OD units.

2.5.3. Alkaline phosphate activity assay

The original extracts and those diluted at ratios of 1/4 and 1/16 were selected for the assessment of alkaline phosphate (ALP) activity. rBMSCs were cultured for 7 days under the same culture conditions as described above. ALP activity was quantitatively determined by an assay based on the hydrolysis of p-nitrophenyl phosphate to p-nitrophenol using the method of Lowry et al [31]. Cells were extracted from the extracts and permeablized with the use of 0.1% Triton X-100 solution (Sigma). Cell lysate from each sample was then used for alkaline

phosphatase assays. The absorbance was measured at 405 nm using a spectrophotometer (UV–VIS 8500, Shanghai, China) and ALP activity was calculated from a standard curve after normalizing to the total protein content. The results were expressed as nanomoles of p-nitrophenol produced per minute per microgram of protein. ALP activity of cells cultured in the medium supplemented with 10% FCS without any addition of extracts served as the control. Data were expressed as mean ± standard deviation (SD). Three independent experiments were carried out and at least five samples per each test were taken for statistical analysis.

A one-way analysis of variance (ANOVA) with Tukey's post hoc test was used for statistical analysis of multiple comparisons. Significant difference was considered when $p < 0.05$.

3. Results and discussion

3.1. Microstructure and mechanical properties of the composites

To achieve reduced biodegradation rates and extended mechanical functionality of magnesium-matrix composites, it is a prerequisite to prepare the composites with minimum microstructural defects, mainly pores, and a homogeneous distribution of bioceramic particles, especially when the volume fraction exceeds 20%. A fabrication technique should be carefully chosen and process conditions must be optimally set, which is challenging, given the pyrophoric nature of magnesium powders with a high affinity to oxygen [32]. We chose a solid-state powder metallurgy route instead of a liquid-state processing route, thereby limiting the reactivity of magnesium during processing and minimizing bulk porosity that would inevitably be introduced by applying casting techniques [32]. **Figure 1** shows the SEM micrographs of the monolithic magnesium, Mg-20% bredigite composite (by volume) and Mg-40% bredigite composite after processing by means of Pressure Assisted Sintering (PAS). The grey dark color and white color in the SEM micrographs correspond to the magnesium matrix and bredigite particles, respectively. These micrographs show highly densified, integrated microstructures and, in

general, homogeneous dispersion of bredigite particles even at an unusually high volume fraction of 40%. It should be noted that achieving such densified microstructures would not be possible by processing at room temperature because of limited ductility of magnesium having an insufficient number of operable slip systems [33]. However, when magnesium is heated above 225 °C, more slip systems become operative, leading to a steep decrease in tensile strength to less than 10 MPa at 350 °C [34]. This suggests that at the pressing temperature used in this study, i.e., 350 °C, the magnesium matrix was considerably ductile, capable of fusing into pores and cavities to fill vacant spots in the microstructure (**Figure 1b** and **c**). With the aid of PAS, the composites with a high volume fraction of bioceramic particles (40 vol.%) could be successfully processed with a minimum amount of porosity. The microstructures of the composites in this research were morphologically different from those of the composites that were prepared by using the extrusion technique. The extruded magnesium-matrix composites were shown to have anisotropic microstructures with ceramic particles being aligned in the extrusion direction [15, 27]. The microstructures of the present composites, however, did not show any dependency on the compaction direction, but were isotropic with spherical Mg powder particles surrounded by homogenously dispersed small bredigite particles (**Figure 1**).

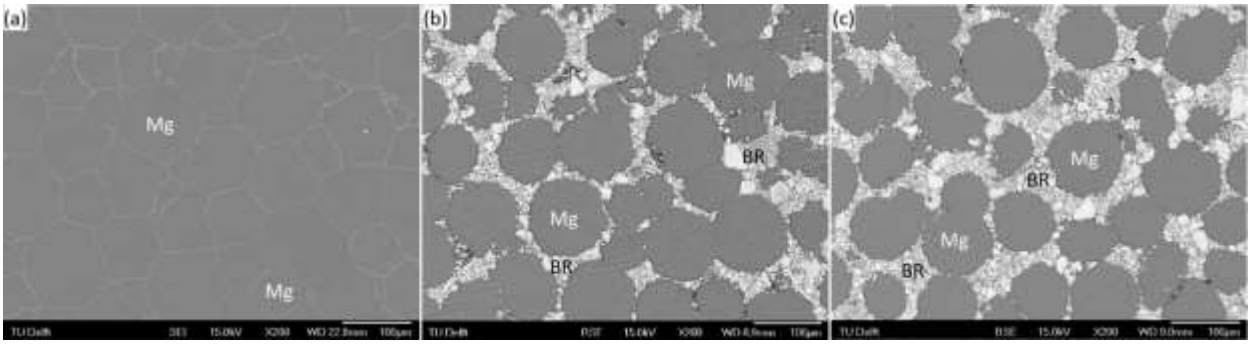

Figure 1. Microstructures of the composites containing (a) 0, (b) 20 and (c) 40 vol.% bredigite particles.

In addition, with the extrusion technique, shear forces, being applied to powder particles during processing, would be much larger than those in PAS and they would introduce additional pores to the microstructure, particularly at metal-ceramic interfaces [27] due to possible microstructure inhomogeneity, such as clustering of ceramic particles [15], mismatch at interface [33] and different deformation mechanisms of metals and ceramics [35]. Thus, the PAS technique would be more appropriate for fabricating Mg-matrix composites with high volume fractions of bioceramic particles (20 - 40 vol.%, being at least 20 % more than most of the Mg-matrix composites previously developed with the extrusion technique [14, 15, 27, 36, 37]). Adding a large volume fraction of (>20 vol.%) of bioactive ceramic particles into the Mg matrix would be highly desirable, because it could significantly reduce the degradation rate of Mg and increase its bioactivity at the same time. The only concern would be the negative influence of ceramic particles on the mechanical behavior of the composites.

Table 1 compares the mechanical properties of the monolithic magnesium and composites with those of the human bone. Adding 20 vol.% bredigite particles to Mg increased the micro-hardness and ultimate compressive strength (UCS) of Mg by 68 and 67%, respectively. The compressive strengths of the composites were comparable to those of the human bone (**Table 1**). The superior mechanical strengths of the composite could be explained by the homogenous dispersion of hard bredigite particles throughout the Mg matrix, immobilizing dislocations and thus causing enhanced resistance to deformation [38-41]. In addition, irregular bredigite particles with multiple sharp edges established stronger interfaces with magnesium by disrupting the pre-existing oxide layer on magnesium powder particles [42, 43] when they were compressed against the matrix during PAS, which contributed to the improved strength and hardness of the composite (**Table 1**). However, a further increase in the volume fraction of bredigite from 20 to 40 vol.% not only did not contribute much to a further improvement of the strength of the Mg-20 vol.% bredigite composite but also deteriorated the ductility (**Table 1**) as a

consequence of the clustering of ceramic particles (bredigite), causing pores and weak bonding among brittle ceramic particles within the clusters and/or between the matrix and clustered particles [44, 45]. The large standard deviations of the mechanical property data of the Mg-40 vol.% composite suggested the relative inhomogeneity in its microstructure, causing its mechanical properties to deviate much more than those of the composite with a smaller volume fraction of bioceramic particles.

Material	Compressive strength (MPa)	Ultimate compressive strength (MPa)	Micro-hardness ($HV_{1.0}$)	Elongation to fracture (%)
Mg	90±3.8	114.27±2.4	38.2±0.1	6.1±0.9
Mg-20% bredigite	135.0±6.2	190. ±6.0	64.05±5.8	13.9±1.8
Mg-40% bredigite	140.0±7.8	192.6±12.2	72.8±9.7	9.8±3.1
Cortical bone [46, 47]	130-180	--	--	--
Femur [48]	167	--	--	--
Tibia [48]	159	--	--	--

Table 1. Mechanical properties of the monolithic magnesium and composites in comparison with the strengths of human's tibia and femur.

The overall porosity of the specimens, being fully densified at the core and semi-porous at the edges, was not larger than 5 % for the Mg-40 vol.% bredigite composite (**Table 2**). Some micro-pores and cracks were observed mostly along the side wall and close to the bottom of cylindrical specimens that were in direct contact with the die during single-action uniaxial hot pressing. During compaction, mixed particles in the bulk under pressure could easily flow, while those at the interface would be locked by a large friction force at the die-material interface. During subsequent ejection, a large friction force at the die-material interface tended to cause

the contacting layer of the specimen to be disintegrated from the bulk. The observed inhomogeneity in microstructure from the core to the surface negatively affected the biodegradation behavior, which will be discussed in the following sections.

Material	Bulk porosity (%)
Mg	0
Mg-20% bredigite	3
Mg-40% bredigite	5

Table 2. Porosity values of the materials PASed at 350 ^{0}C.

3.2. Degradation rates of the composites

Figure 2 shows the degradation profiles of the composites and the accompanied pH changes during immersion in DMEM over different times up to 12 days, in comparison with those of the monolithic magnesium also prepared from the powder. It should be noted that the mass loss values of all the samples before 24 h of immersion were converted from the measurements of hydrogen evolution because the mass loss measurements were inaccurate at low degradation rates in the first phase of immersion. The other data points were directly taken from mass loss measurements. From **Figure 2**, it is clear that all the samples degraded very slowly during the first 24 h and then degradation accelerated until day 6 and decelerated from day 6 to day 12. Despite the similar trends of degradation between the monolithic magnesium and the composites, the former was completely corroded by day 12, causing intense alkalization of the solution to reach a pH value of 9.8, despite the presence of HEPES as a pH buffer (see the black dashed line in **Figure 2**). The average degradation rate of the monolithic magnesium

(**Table 3**), i.e., 31.41 mg/cm^2/day determined by measuring the mass loss after 12-day immersion per 1.33 cm^2 of the exposed area, was in good agreement with that determined in previous studies on cast magnesium specimens (19-44 mg/cm^2/day) [11]. By contrast, the Mg-20% bredigite and Mg-40% bredigite composites had markedly reduced average degradation rates of 1.26 and 2.65 mg/cm^2/day, respectively. Thus, a substantial reduction in degradation rate by up to a factor of 24 was achieved by adding bredigite particles to magnesium.

Material	Degradation rate (mg/cm^2/day)
Mg	31.41
Mg-20% bredigite	1.26
Mg-40% bredigite	2.65

Table 3. Calculated average degradation rates of the materials after 12 days of immersion in HEPES-buffered DMEM.

The degradation of the composites was slower than that of cast ZE41 and AZ91 alloys at average dissolution rates of 7.71 and 6.95 mg/cm^2/day in buffered Hank's solution, respectively [49]. According to the literature, the amount of Mg^{2+} released from the bredigite-containing magnesium-matrix composites is tolerable for the body (19–44 mg/cm^2/day, as long as the total surface area of a magnesium implant is less than 9 cm^2) although the amount of the equivalent hydrogen evolution for such a mass loss is still not tolerable for the body (tolerable level: 0.01 ml/cm^2/day) [11]. A distinct advantage of the magnesium-matrix composite with a large volume fraction of bredigite particles lies in a reduced amount of liberated hydrogen, which is not equivalent to the total mass loss anymore, because partial dissolution of bredigite particles also contributes to the total mass loss. In other words, because partial dissolution of bredigite particles does not produce additional hydrogen, the overall gas evolution of the composite would be less than monolithic Mg, having the same exposed area. For example, the Mg-20%

bredigite composite that loses weight at a rate of 1.26 mg/cm^2/day theoretically liberates hydrogen gas at a rate of 1.01 ml/cm^2/day, which is 0.25 ml/cm^2/day less than the monolithic magnesium having the same weight at the start of immersion.

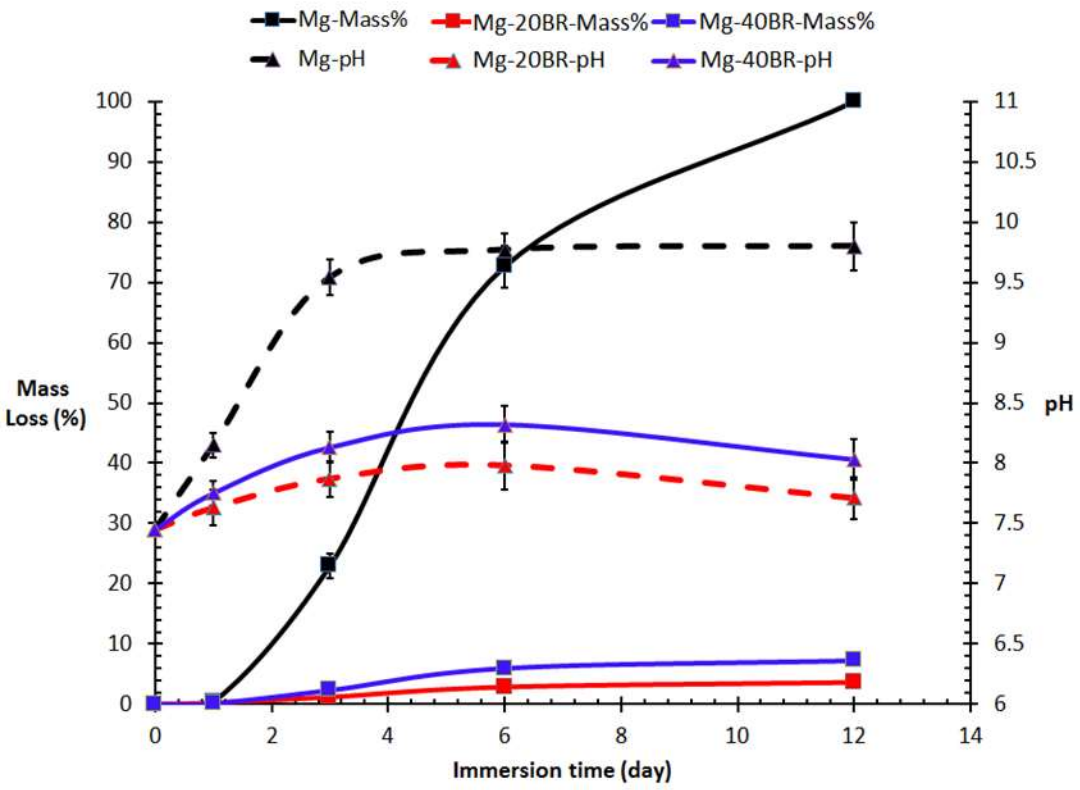

Figure 2. Mass losses and pH changes of the materials during immersion in DMEM for 12 days.

3.3. Electrochemical degradation of the composites

3.3.1 Open circuit degradation of the composites

When magnesium is exposed to water, it quickly oxidizes to form magnesium cations (Mg^{2+}) by giving up two valence electrons (**Equation 1**). Water on the other hand takes up free electrons at cathodic sites and chemically reduces to hydroxyl anions and hydrogen gas (**Equation 2**). With the accumulation of Mg^{2+} ions in the solution, there will be more cations reacting with OH^- groups to form $Mg(OH)_2$ that has a low solubility (12 mg/l) in water and precipitates out in the medium eventually [50, 51].

$Mg_{(s)} \rightarrow Mg^{2+}_{(aq)} + 2e^-$ Anodic reaction (1)

$H_2O_{(l)} + 2e^- \rightarrow OH^-_{(aq)} + H_{2(g)}$ Cathodic reaction (2)

$Mg^{2+}_{(aq)} + 2OH^-_{(aq)} \rightarrow Mg(OH)_{2(s)}$ Product formation (3)

A $Mg(OH)_2$ layer formed on the magnesium surface (**Equation 3**) may be thought to act as a barrier against further dissolution by preventing mass diffusion between the magnesium substrate and the solution [52]. In electrochemistry, the formation of this layer shifts the Open Circuit Potential (OCP) of magnesium to more positive values [53]. OCP value evolutions of the monolithic magnesium and the composites over 24 h are presented in **Figure 3**. The slopes of the OCP curves, indicative of the rates, at which the surface layer formed over time, were similar during the first hour of immersion. However, the differences became larger as degradation proceeded from 1 to 24 h. **Figure 3** shows that in the case of the monolithic magnesium a surface layer was rapidly formed. Solution alkalization, which occurs along with magnesium dissolution, encourages the formation of a partially protective hydroxide layer (**Equation 3**). In the case of the composites, however, the rate of the surface layer formation became lower with increasing volume fraction of bredigite particles (**Figure 3**). Considering the fact that bredigite particles were present in the composites at the expense of the magnesium matrix on the whole surface, the delayed and incomplete development of a hydroxide surface layer on composite samples could be due to their low ability to reach a certain degree of solution alkalinity (**Figure 2** - dashed lines). It also indicated that within 24 h bredigite particles did not positively contribute to surface passivation.

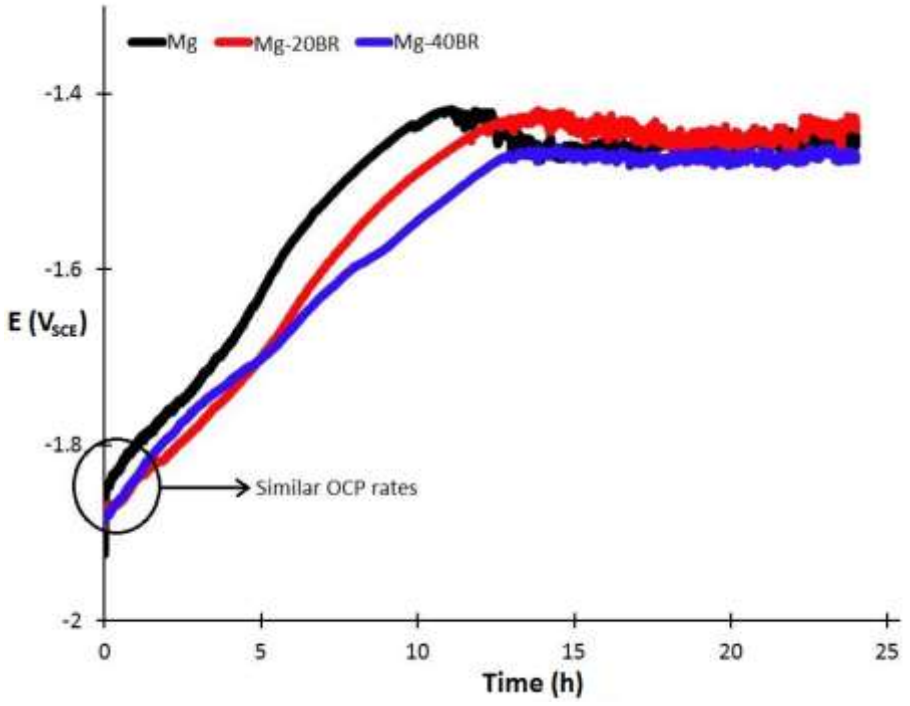

Figure 3. Open Circuit Potential (OCP) curves of the materials immersed in HEPES-buffered DMEM for 24 h.

The question as to if bredigite really participated in the degradation process during the first 24 h could be answered by detecting silicon in the solution and in the surface layer, because only bredigite contains this element. EDS point scans could not identify the presence of silicon in the surface layer of corroded samples. Furthermore, ICP analysis (**Figure 4**) showed very limited amounts of silicon, i.e., less than 3 ppm in the solution after one day of immersion, meaning that bredigite stayed almost inert during the first day of immersion, thus not contributing to the chemistry of the surface layer by dissolving. It confirmed that the partially protective surface layer was mainly formed during the first 24 h due to the chemical interaction between the magnesium matrix and DMEM. Thus, monolithic magnesium samples, having a larger exposed magnesium surface area as compared to composite samples, could form a homogenous,

complete surface layer more quickly than the composites (**Table 4**) as a result of a greater extent of interaction between magnesium and DMEM.

Material	Stabilization potential E_s (V_{SCE})	Elapsed time till stabilization T_s (h)
Mg	-1.43	10.56
Mg-20% bredigite	-1.44	12.48
Mg-40% bredigite	-1.47	13.01

Table 4. Surface stabilization potentials and elapsed times for the materials immersed in HEPES-buffered DMEM.

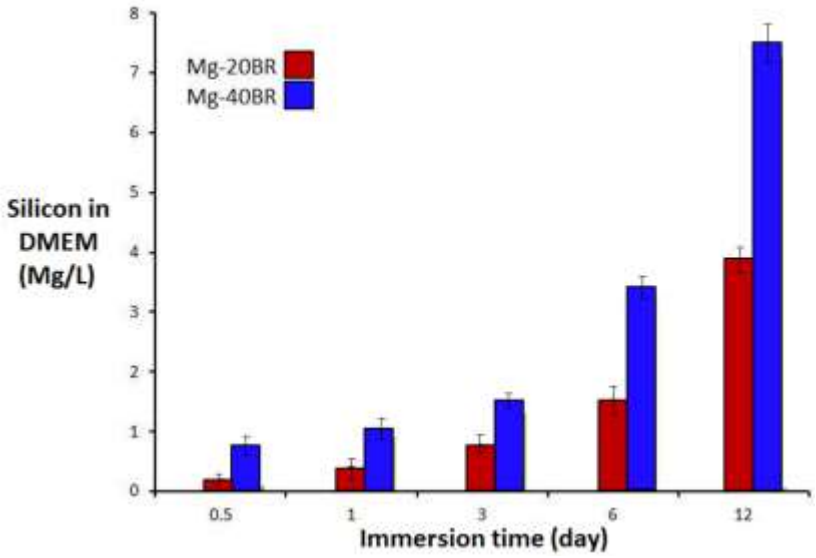

Figure 4. Concentrations of silicon released from the composites to DMEM as a function of immersion time.

3.3.2. Degradation under forced polarization conditions

Potentiodynamic polarization (PDP) curves of the composites at 1 and 24 h of immersion (**Figure 5a-d**) showed an almost 230 mV increase in corrosion potential *E* (V_{SCE}) (visible by comparing the corrosion potentials in **Figure 5a** to the ones in **Figure 5c**) as a result of the gradual formation of a partially protective surface layer along with immersion time. The gradual formation of the surface layer caused the cathodic activity of all the samples to decline within 24 h (**Figure 5b** and **d**, from 0 to 250 s). This suggested that the formation of a surface layer inhibited water reduction on the magnesium surface. On the other hand, the anodic activity of samples remained almost unchanged, despite the presence of the surface layer (**Figure 5b** and **d**, from 250 s onwards), meaning that the formation of the surface layer exerted a smaller impact on the anodic activity than on the cathodic activity. This could be because anodic currents were derived from several highly intense anodic regions, occupying a relatively small proportion of the scanned area, while cathodic values were obtained from a much larger fraction of the working area [54]. In addition, the number and intensity of the local anodes were shown to increase with time in proportion to the area of the exposed local cathode [54]. In other words, localized corrosion in composite samples progressed under cathodic control. Thus, pH, affected by the cathodic reaction, must have had a significant effect on the magnitude of the corrosion current. It was found earlier by the present authors that in buffered solutions the cathodic and anodic current densities in the PDP tests were higher than those in DMEM without the buffer and the OCP values were more negative than those in DMEM without the buffer due to the pH maintenance effect of the buffer [6].

At anodic over-potentials, both the monolithic magnesium and the composites went through surface breakdowns, which is visible from a sudden increase in corrosion current (**Figure 5a** and **b** - indicated by arrows), meaning that pitting corrosion took place as one of the corrosion mechanisms involved.

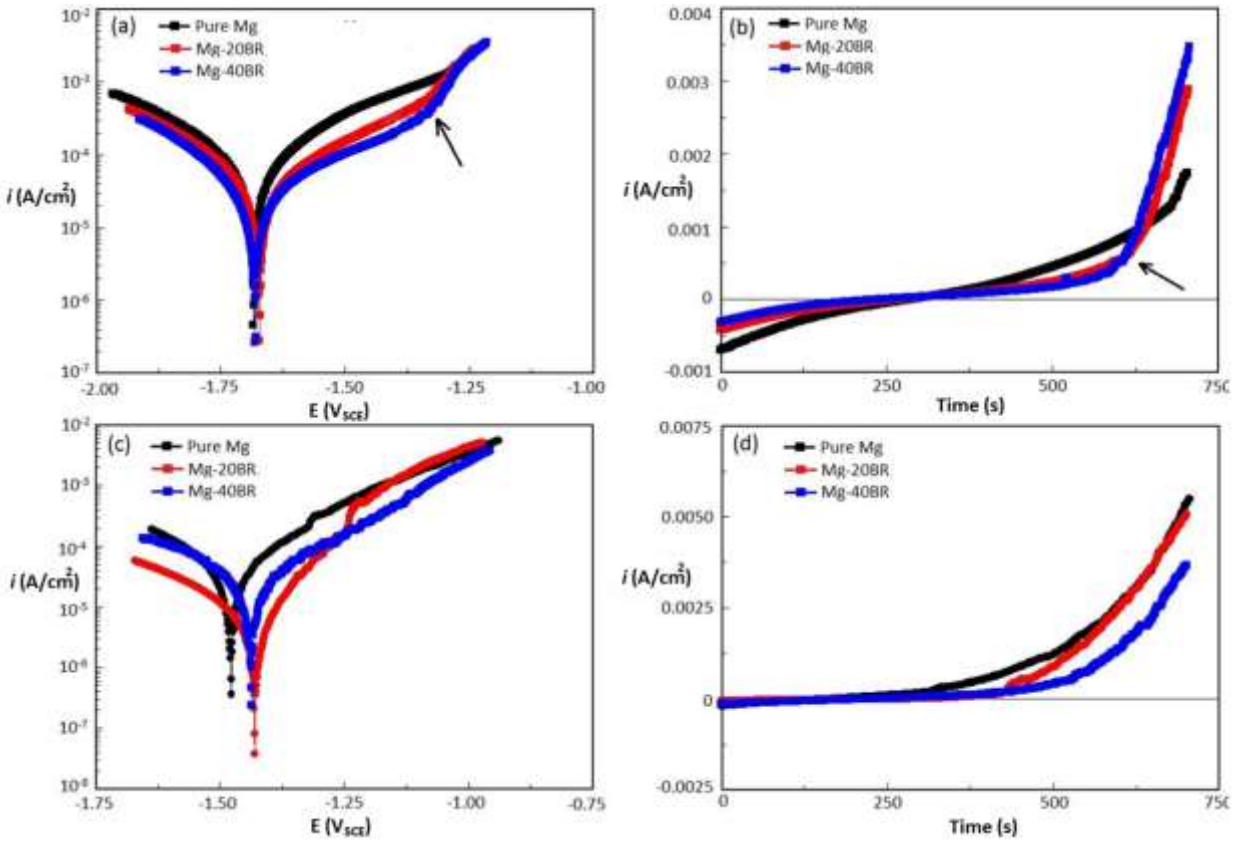

Figure 5. Potentiodynamic polarization (PDP) curves at 1 h (a and b) and 24 h (c and d) of immersion. Note that during the PDP tests the OCP changed with exposure time from 1 to 24 h (Figure 5a and c); the same potential range of 0.7 V from -0.2 V_{OCP} to 0.5 V_{OCP} was applied at both exposure times.

3.4. Degradation mechanisms of the composites

3.4.1. Homogenous volumetric degradation

SEM micrographs of corroded samples (**Figure 6a-f**, corresponding to an immersion time of 0.5 day) showed that the dissolution of monolithic magnesium samples and that of the magnesium matrix in composite samples mostly proceeded through pathways along grain and prior powder particle boundaries. Grain boundaries are known as the distorted areas with high internal

energy, as compared to the grain interior, and can be regarded as an area of defects in the crystal structure with a configuration of dislocations and crystal lattice mismatch. It is well known that anodic metal dissolution will be accelerated in the vicinity of dislocations [56]. In our previous study on magnesium made from powder, it was observed that grain and prior power particle boundary dissolution occurred quickly after 15 s immersion, causing nano-cracks, less than 100 nm long, to appear on the surface [6]. These nano-cracks grew fast in size, up to 500 times larger than the initial length within one hour. The further development of the surface crack-like features created an interconnected network of surface cavities, propagating transversely (**Figure 7**) over the surface and longitudinally into the surface, which brought the electrolyte (DMEM) in contact with the fresh surface, causing further dissolution. Because the surface crack-like features, or in other words, grain and prior powder particle boundaries were distributed evenly on the surface, it resulted in homogenous dissolution of the magnesium matrix, as shown in **Figure 7a**. The cross-section micrograph of the Mg-20% bredigite composite after six days of immersion in DMEM revealed a homogenous inward development of the dissolution front, as the magnesium matrix was transformed into the hydroxide form [56]. The inward development of the corrosion layer was confirmed by the presence of trapped, undissolved bredigite particles within the transformed layer after six days of immersion. Therefore, grain and prior powder particle boundary corrosion that initiated immediately after immersion provided a homogenous slow pattern of degradation through the volume. Given that the thickness of the transformed layer was approximately homogenous (**Figure 7a**), the general degradation rate, mainly determined by grain and prior powder particle boundary dissolution, excluding pitting corrosion, could be calculated by measuring the average thickness of the surface layer at a given time of immersion, which resulted in an average degradation rate of 0.43 $mg/cm^2/day$ for the Mg-20% bredigite composite. A similar degradation rate was calculated for magnesium samples, tested in DMEM and in McCoy's 5A-5% Fetal Bovine Serum (FBS) medium [57, 58]. This calculated degradation rate is considerably lower than the average

degradation rate determined from the mass loss (**Figure 2**), suggesting that another corrosion mechanism must have played a more decisive role. In other words, grain and prior powder particle boundary dissolution was only one of the active degradation mechanisms and due to its slow rate, it could not be responsible for the total disintegration of magnesium samples with a mass of 3 g in twelve days (**Figures 2 and 6**).

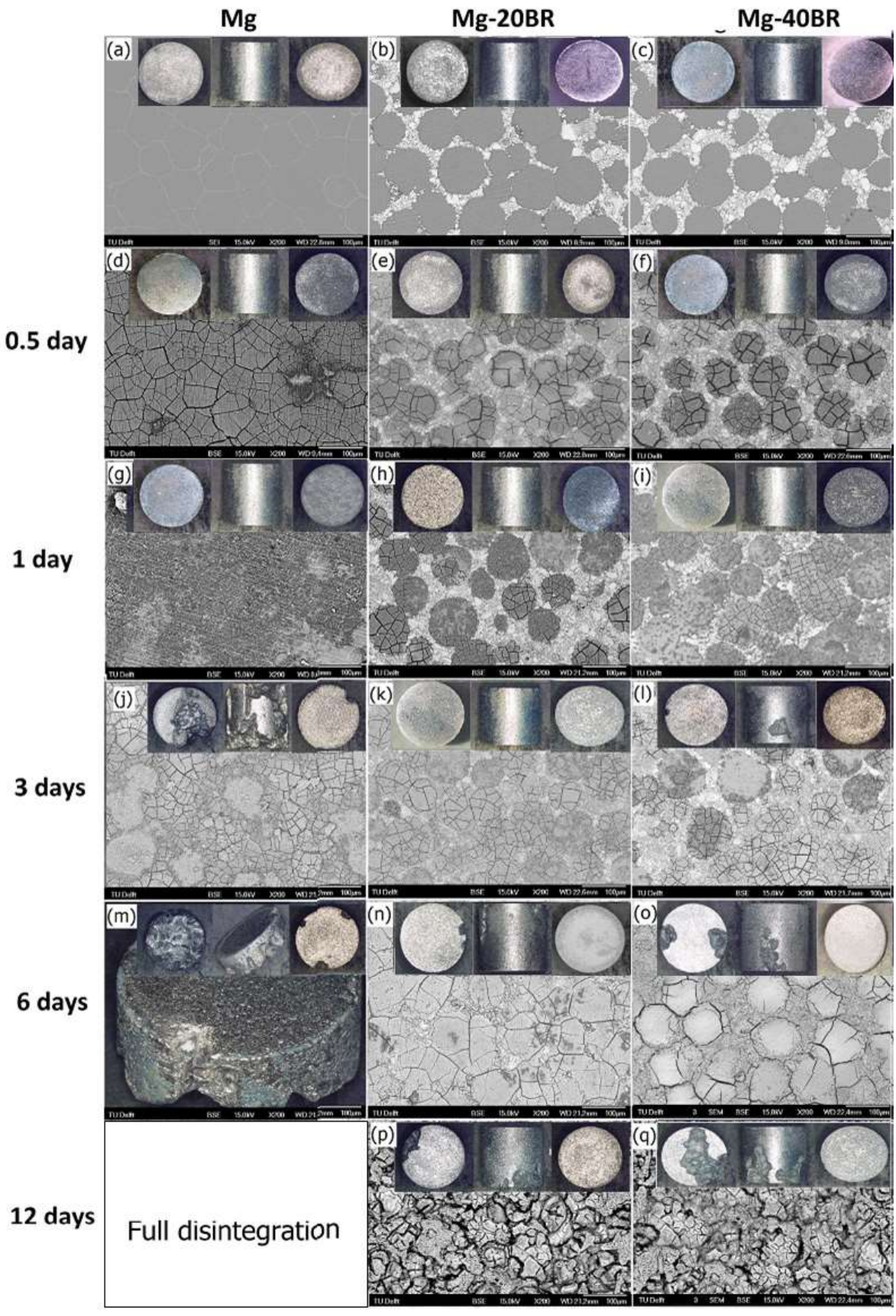
Mg
Mg-20BR
Mg-40BR
0.5 day
1 day
3 days
6 days
12 days
(a)
(b)
(c)
(d)
(e)
(f)
(g)
(h)
(i)
(j)
(k)
(l)
(m)
(n)
(o)
(p)
(q)
Full disintegration

Figure 6. SEM back-scattered micrographs of the materials containing 0 (the first column), 20 (the second column) and 40 vol.% (the third column) bredigite particles, showing different responses of these materials to DMEM during immersion through a period of 12 days. The insets represent bottom, side, and top of the samples from left to right.

3.4.2. Localized pitting corrosion

Pitting was another phenomenon observed in corroded samples (**Figure 6g-n** - the insets). In the preceding subsection on the electrochemical tests, the sudden increases in corrosion current density, mostly at anodic overpotential (**Figure 5b**, indicated by the arrow), indicated the formation of early pits. These pits appeared within the first three days of immersion and grew into large corrosion cavities, appearing mostly on the side walls and bottom of samples, while the top surface of these samples remained intact (**Figure 6g-n** - the insets). This could be due to the presence of structural disintegrity and cracks at the edges of samples formed during ejection subsequent to PAS, as discussed earlier. When samples were immersed in DMEM, the bulk matrix became undermined as pits (or cracks) provided feeding pathways for the corrosive medium to move forward through the anodic dissolution of crack tips [59]. Earlier studies on magnesium parts processed through the powder metallurgy route also indicated higher dissolution of samples mostly at the edges, because of the presence of disintegrity introduced during the material processing [57]. Pitting corrosion caused the degradation rates of all the samples to exceed the degradation rate due to grain and prior powder particle boundary corrosion (*i.e.* 0.43 mg/cm^2/day) by a factor of 73, 2.93 and 6 for the monolithic magnesium, Mg-20% bredigite and Mg-40% bredigite composites, respectively. It is thus clear that pitting corrosion, once initiated, plays a more important role than the grain and powder particle boundary degradation mechanism and dominates the degradation process. In addition to the edge effect, the presence of impurities beyond their tolerance limits may have contributed to

pitting corrosion as well. XRF analysis of the magnesium powder used, having a purity of 99.86%, revealed 320 and 160 ppm of iron and nickel, respectively, which were higher than their tolerance limits (170 and 5 ppm, respectively) [60]. These impurities have very low solubility limits in the magnesium solid solution, leading to precipitation after solidification or PAS mostly along the grain boundaries. The precipitates generate strong micro-galvanic coupling with magnesium, causing intensive anodic dissolution of the magnesium solid solution in the vicinity of the precipitates.

When pitting occurs, the degradation rate is expected to decline after a while, since the dissolution process produces an alkaline environment that will stabilize magnesium hydroxide as a protective surface layer. However, in monolithic magnesium samples, pitting corrosion occurred at the beginning of immersion and even accelerated in alkaline environments (pH between 8 and 8.9, **Figure 2**). It suggested that once early pits were initiated, they could autonomously grow, showing no sign of passivation. The PDP curves also indicated that surface passivation did not effectively take place after the surface breakdown as the corrosion currents in all the samples increased with time (**Figure 5b** - arrow). Pitting is basically an intensive anodic dissolution process, leading to the accumulation of magnesium cations in the solution next to the corroding surface. In this manner, hydrolysis of magnesium cations with water will be possible [6, 61, 62], resulting in the formation of hydrogen protons, acidifying the anodic regions (**Equation 4**).

$$4Mg^{2+}_{(aq)}+4H_2O_{(l)} \rightarrow Mg_4(OH)_4{}^{4+}_{(aq)}+4H^+_{(aq)} \quad (4)$$

The formation of hydrogen protons is catastrophic to the degradation of the magnesium matrix, because it can directly attack the hydroxide layer, producing water and magnesium cations, as expressed in **Equation 5**.

$$Mg(OH)_{2\,(s)} + 2\,H^{+}_{(aq)} \rightarrow 2\,H_2O_{\,(l)} + Mg^{2+}_{\,(aq)} \quad (5)$$

The products of hydrogen attack (**Equation 5**) can be consumed in the hydrolysis reaction (**Equation 4**), acidifying the region again. In addition, hydrogen protons together with magnesium cations electrostatically attract chloride ions to the region, producing hydrochloric acid attacking the substrate, producing highly soluble $MgCl_2$ and hydrogen gas (**Equation 6 and 7**).

$$Mg_{\,(s)} + 2HCl_{\,(aq)} \rightarrow MgCl_{2\,(aq)} + H_{2\,(g)} \quad (6)$$

$$Mg(OH)_{2\,(s)} + 2Cl^{-}_{(aq)} \rightarrow MgCl_{2\,(s)} + 2OH^{-}_{(aq)} \quad (7)$$

The above mentioned reactions indicate that once pits get initiated, the magnesium matrix cannot re-establish a protective layer, leading to self-driven intense pit development, and finally to the total disintegration of cylindrical magnesium samples by day 12 despite the high level of alkalinity (**Figure 2**). In the case of the composites, a second phase with more resistance to H^+- and Cl^--driven attacks, such as bredigite, can limit the intense pit propagation by blocking pitting pathways, giving time to the matrix to re-establish a surface layer. The cross section of corroded composite samples after 6 days of immersion in DMEM indeed showed the blocking of pitting pathways by bredigite particles, once the inwardly developed pit front reached these particles (**Figure 7b**). The remainders of bredigite particles within the body of the surface layer appeared to be partially dissolved ones, meaning that they degraded at a slower rate than the magnesium matrix.

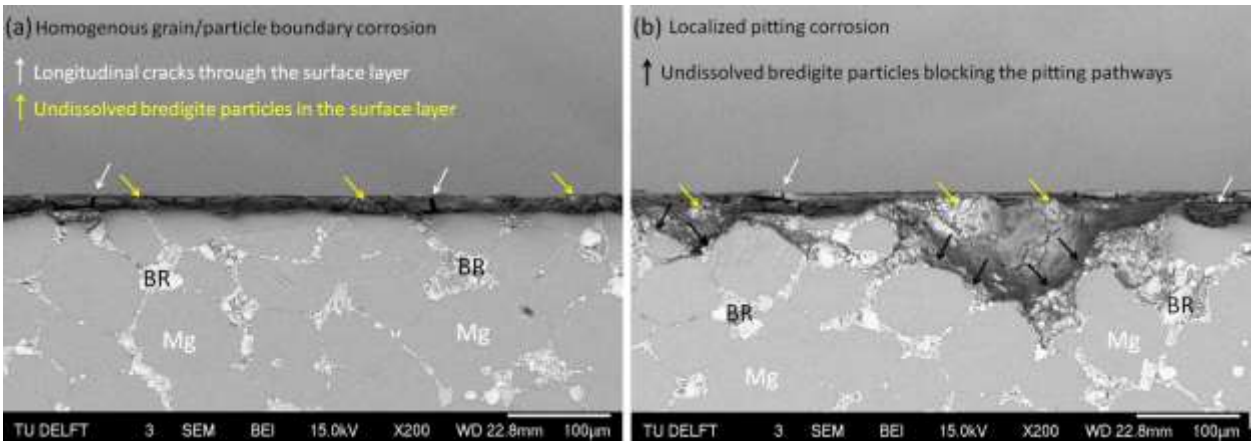

Figure 7. SEM back-scattered images of the cross section of Mg-20% bredigite composite samples after 6 days of immersion. (a) shows the homogenous development of the corrosion layer. (b) shows the bredigite particles blocking pitting pathways across the magnesium matrix.

3.4.3. Surface morphology and chemistry of corroded composite samples

The initial hydroxide layer showed an island-like feature because of the longitudinal and transversal surface cracks that separated the islands (**Figure 6d-f**). **Figure 8** shows the co-existence of phosphorus (from DMEM) along with calcium and silicon on the corroding surfaces of the composites. Bioactive behavior initiates when these ions react with each other and/or react with other ions, originating from DMEM, such as calcium and phosphate ions, producing insoluble inorganic compounds precipitated on the surfaces (**Figure 8** and **Figure 9**).

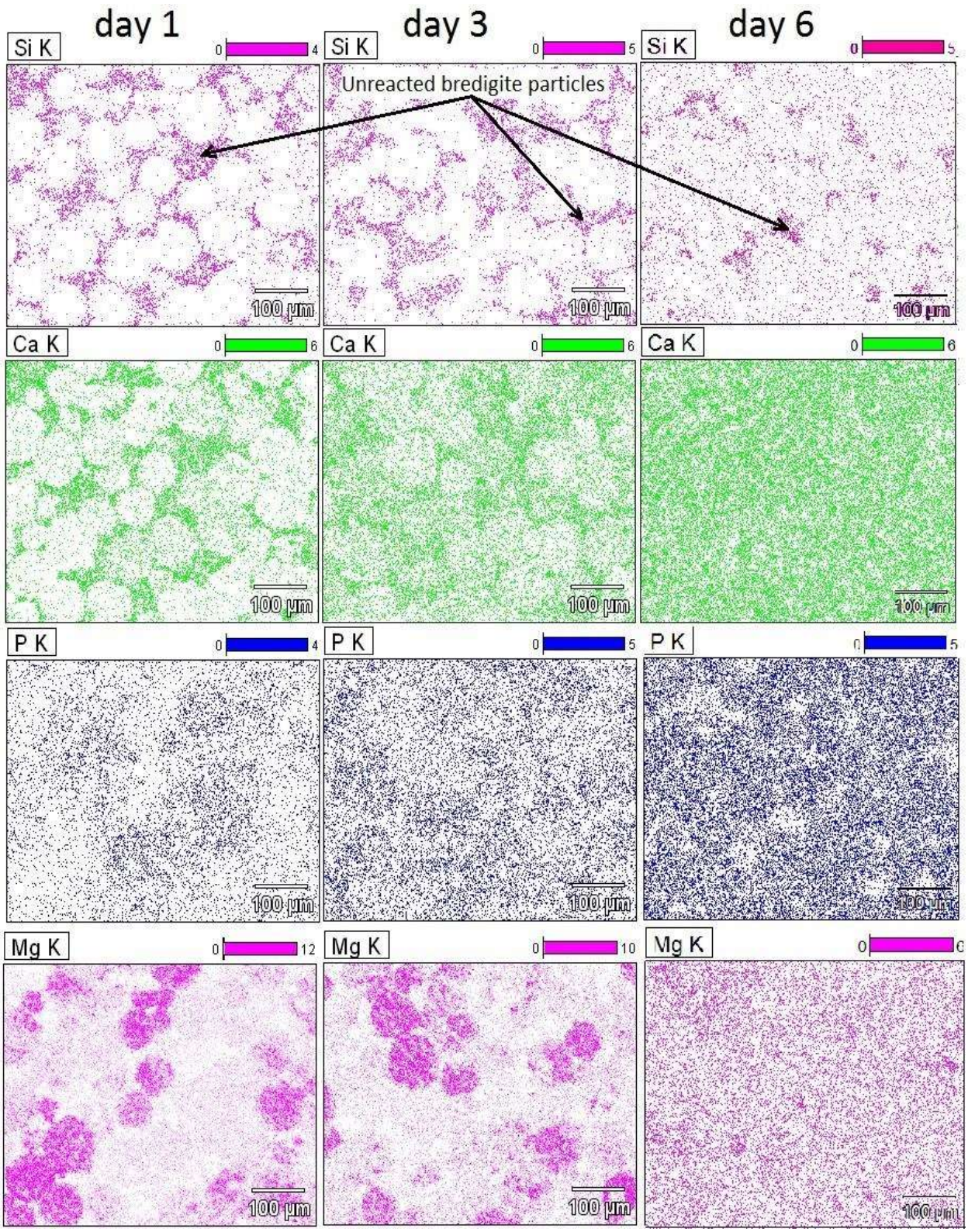

Figure 8. EDX elemental mapping of the composite containing 40 vol.% bredigite particles, showing the gradual precipitation of Si, Ca and P on the surface as a function of immersion time.

Phosphate ions preferentially bond with Ca^{2+} and Mg^{2+} [19] to form white compounds of magnesium-containing apatite on the corroding surfaces (**Figure 7d-i** and **Figure 9**). The involvement of magnesium in calcium phosphates as a corrosion layer decreases the degree of crystallinity and enhances the degradation rate of calcium- and phosphate-containing compounds, which, as compared to HA, brings about better bioactivity [63]. Mg-CaP is essential for exhibiting good biocompatibility and bioactivity because proteins, such as fibronectin and vitronectin that act as cell attachment–promoting proteins, can be better adsorbed in the presence of Ca-Mg-P precipitates [64]. The initial Mg-CaP-containing layer, appearing as the white spots embedded in the gray-colored hydroxide layer (until day 3 - **Figure 6g-l**) gradually expanded over the whole surface until it fully covered the surface, thus appearing as a white Mg-CaP-containing layer (6^{th} day-**Figure 6n** and **Figure 9**). The relative amount of phosphorus deposition was observed to be larger on the magnesium matrix (~11 at.%) than on bredigite particles (2.61 at.%) by day 3 of immersion (**Figure 8**). This is mainly because the magnesium matrix dissolves faster than bredigite particles and the local pH value will be raised near the corroding magnesium surface, possibly well above 10 [6], thereby encouraging the precipitation of Ca- and P-containing phases [56].

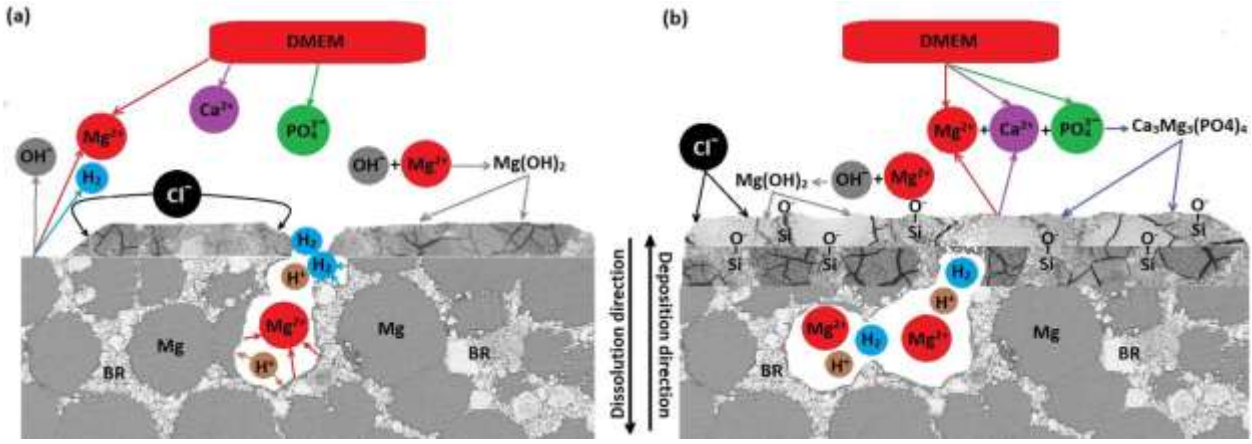

Figure 9. Schematic of the biodegradation process of the composites after 1 day (a) and 6 days (b) of immersion in DMEM.

Element mapping on composite sample surfaces showed negligible deposition of silicon by day 3 (**Figure 8**). However, its involvement in the surface layer, yet below 1 at.%, was identified by day 6 and 12 of immersion. One reason for relatively low silicon deposition is that calcium ions from bredigite are released preferentially to silicon ions by ion exchange with H^+ [65]. Thus, most of silicon in bredigite would stay within the unreacted part, forming a negatively charged surface with the functional group ($\equiv Si - O^-$) [65], which electrostatically attracts magnesium and calcium cations (**Figure 8** and **9**). Some colonies of silicon visible on the surface after 6 days of immersion (**Figures 8** and **9**) were actually the un-reacted parts of the ceramic retained within the body of the corrosion layer. Thus, by day 12, the simple hydroxide surface layer was transformed into a compact mixture of unreacted bredigite particles embedded within a layer of Mg, Ca, P and Si-containing compounds (**Figure 9**).

With the addition of the HEPES buffer to DMEM, the local pH close to the magnesium surface could be largely maintained, which would result in slower formation of a surface hydroxide layer as well as faster progression and more intensive micro galvanic activities [54]. In addition, the tendency of calcium phosphates to precipitate from the HEPES-buffered DMEM solution would be significantly reduced, as the local pH of the solution was maintained at a relatively low level by the buffer [6, 66]. In other words, degradation rates derived from this research would have been lower and calcium phosphate precipitation would have been more intensive if the buffering agent had not been added to DMEM.

3.5. Mechanical properties of the composites in relation to biodegradation

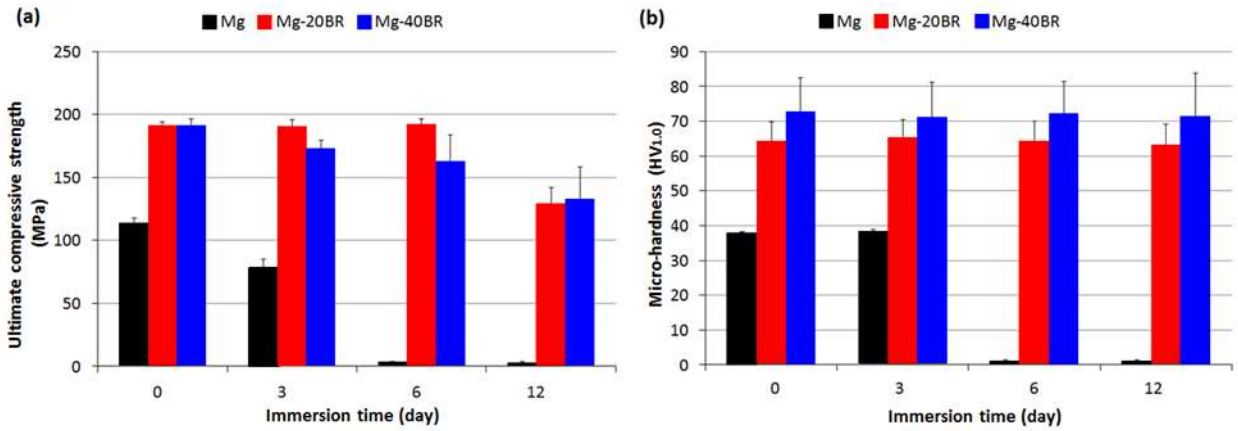

Figure 10. Ultimate compressive strength (a) and micro-hardness (b) of the composites as a function of immersion time in DMEM.

Degradation of the composites in DMEM affected their mechanical behaviour, causing the UCS to decrease gradually from 190 MPa to about 130 MPa in 12 days. **Figure 11** shows that mechanical cracks were preferably initiated at the corrosion pits during compression tests, deteriorating the mechanical strength as well as the ductility of the composites. On the other hand, there were no significant differences between the micro-hardness values, before and after immersion in DMEM (**Figure 10b**). In the previous section we showed that pitting corrosion, as the dominant mechanism of degradation, mostly initiated at the edges of the sample and its penetration towards the core was limited by the blocking effect of bredigite particles. Thus, the core of the samples would still remain intact and thus showed the same values of micro-harness as before the immersion tests. The gradual loss of the compressive strength was also related to preventing the pitting corrosion from reaching the core of the samples.

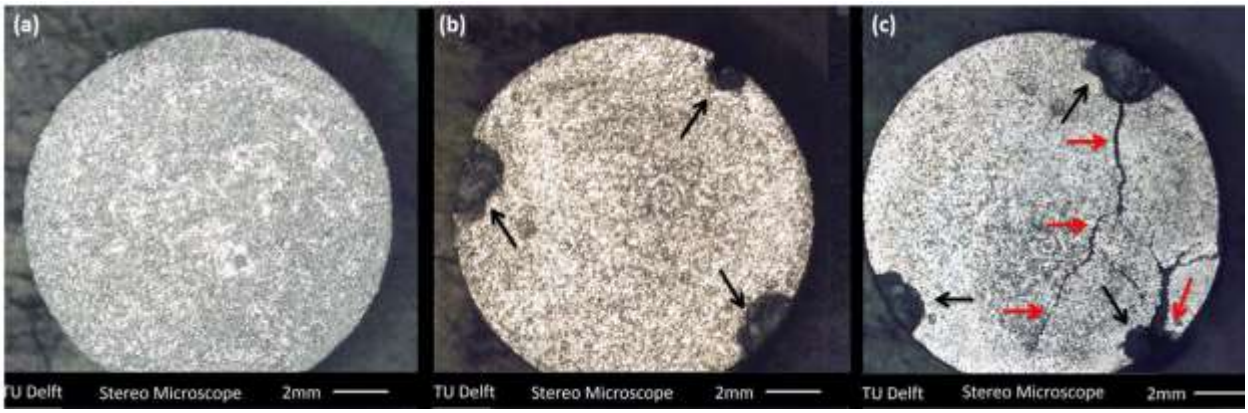

Figure 11. Morphologies of the Mg-20% bredigite composites before immersion (a), after immersion for 12 days (b) and after the compression tests (c), showing corrosion pits (black arrows) and mechanical cracks initiating at the pits (red arrows).

The mechanical properties of the composites after 12 days of immersion in DMEM were still in the range of those of femur and tibia (**Table 1**), confirming the mechanical functionality of the composites within the first two weeks of implantation. Our positive results on the short-term mechanical tests warrant further investigations on the degradation behaviour and mechanical properties of the composites in the *in vivo* situations.

3.6. Biocompatibility and bioactivity of the composites in relation to biodegradation

3.6.1 Cell attachment

The morphologies of rBMSCs seeded on pure Mg and Mg-20% bredigite composite samples after incubation for 6 h are presented in **Figure 12**. It is clear that the cell morphology on the Mg-20% bredigite composite (**Figure 12b**) differed from that on pure Mg (**Fig. 12a**). The filopodia of the cells attached on pure Mg were hardly discernible. By contrast, the Mg-20% bredigite composite showed an enhanced ability of early cell attachment, as evidenced by the appearance of cytoplasmic extensions.

It is widely accepted that cell attachment is a desirable cellular response at the cell-material interface, as it promotes the cellular response to the implant surface [67]. However, pure Mg possesses a poor ability to support cell attachment due to extensive evolution of H_2 bubbles and rapid elevation of pH at its surface, which results in a hostile surface microenvironment, thereby inhibiting the attachment of cells [68]. In the present study, it was clear that the presence of bredigite in the composite led to improved cell attachment as compared with pure Mg. On the one hand, the enhanced cell attachment could be related to the fact that the degradation of the composite was significantly lower than that of pure Mg, which would result in much less H_2 evolution and lessened surface pH increase, thus presenting a more favorable surface condition for cellular response. On the other hand, the fast Ca-P deposition induced by the presence of bredigite (although not as a compact layer) [23], might have helped improve the initial cell attachment, as demonstrated in previous studies [68,69]. The exact mechanism, however, is still unclear and worth further investigating in our follow-up studies. Nevertheless, it is reasonable to assume that, with an enhanced ability to support cell attachment, the Mg-20% bredigite composite would exhibit superior performance as compared with pure Mg, especially at the early stage right after implantation.

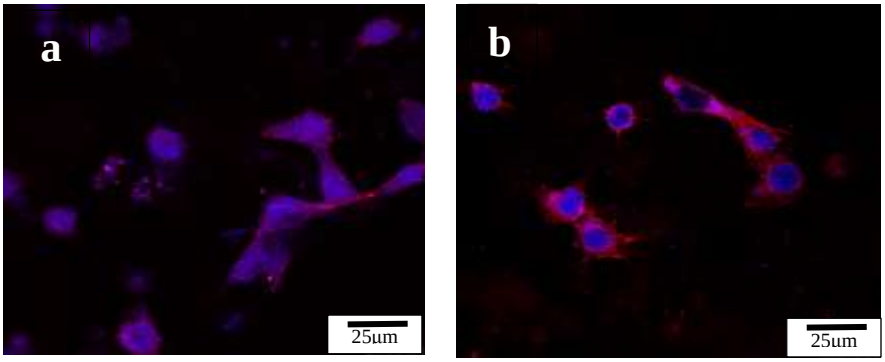

Fig. 12 Confocal microscopy images of the surfaces of pure Mg (a) and Mg-20% bredigite composite (b) samples after cell seeding for 6 h.

3.6.2 Cell proliferation and differentiation in the presence of the ionic products from the materials

A high degradation rate of magnesium causes the accumulation of ionic products in the vicinity of the corroding surface. In *in vitro* situations, the proliferation of cells is closely related to the ionic environment of the culture medium [70]. For Mg-based materials designed for biomedical applications, the extracts of the samples after a certain time of immersion in a corrosive solution are collected and then stored at 4°C prior to the cytotoxicity test, which is known as the indirect cytotoxicity test [27, 71-77]. The extraction procedure is often conducted in the DMEM solution [75-78], which closely mimics the chemical composition of the blood plasma [79]. Our results from the indirect cytotoxicity tests on monolithic Mg samples confirmed that cell proliferation was significantly inhibited by the original (undiluted) magnesium extracts, whereas diluting the extracts led to enhanced proliferation of cells (**Figure 13a**).

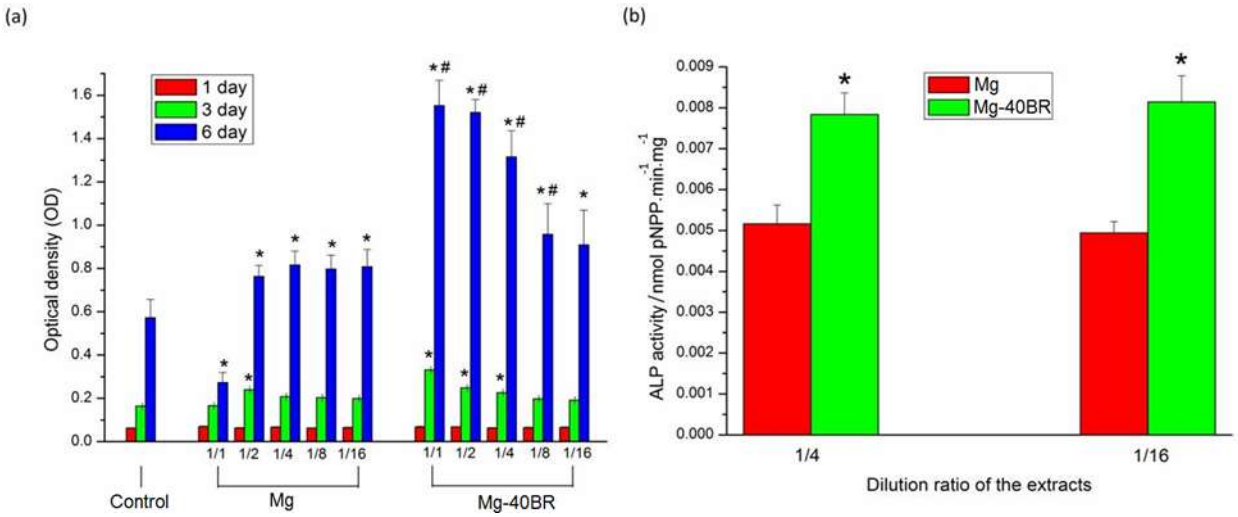

Figure 13. (a) MTT assay of rBMSCs cultured in monolithic magnesium and Mg-40%bredigite extracts at different dilution ratios. The ratio of 1/1 stands for the original extract without diluting. The symbols * and # represent significant difference ($p < 0.05$) as compared with the control and with the magnesium extract, respectively. (b) ALP activity of rBMSCs in the presence of monolithic magnesium and Mg-40% bredigite composite extracts at the dilution ratios of 1/4 and

1/16. The asterisk (*) indicates that the ALP activity of the Mg-40% bredigite group was significantly higher than that of the magnesium group ($p < 0.05$).

In contrast to the monolithic magnesium group, the extracts of the Mg-40% bredigite composite exhibited much higher abilities to stimulate the proliferation of rBMSCs. Considering the fact that magnesium ion concentrations in the extracts of the Mg-40% bredigite composite and those after dilution were lower than those in the magnesium group (**Figure 14**), the stimulatory effect could only be attributable to the presence of silicon ions that were released from the bredigite component inside the composite material. Previous studies showed that silicon-containing ionic products from the degradation of silicate-based ceramics stimulated cell proliferation [70, 80]. It should be noted that for the Mg-40% bredigite composite, there might be a synergistic effect of silicon and magnesium ions on the proliferation of cells, as indicated by the previous studies on Ca-Mg-Si bioceramics including bredigite [25]. This inference needs to be confirmed in further investigation. Nevertheless, it is clear that the incorporation of bredigite into the magnesium matrix could lead to stimulated cell proliferation and thus enhanced bone regeneration, which is highly desirable for the clinical application of biodegradable implants [81].

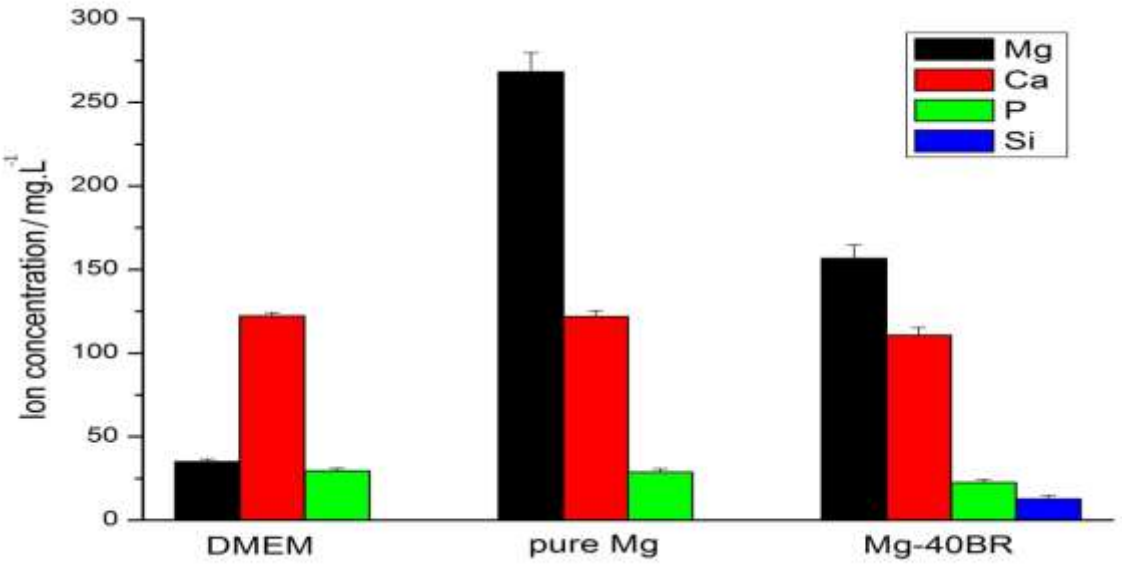

Figure 14. Concentrations of ionic products in composite extracts after 24 h of immersion.

The osteogenic differentiation of rBMSCs was investigated using an ALP assay on magnesium and Mg-40% bredigite extracts at dilutions of 1/4 and 1/16, and the results are presented in **Figure 13b**. A quantitative study showed that Mg-40% bredigite composite extracts induced a higher ALP activity than the magnesium group. Further comparison between Mg-40% bredigite extracts with different diluting ratios, namely 1/4 and 1/16, revealed that the differences between the ALP activities of cells in these groups were not statistically significant ($p > 0.05$).

Osteogenic differentiation of BMSCs is one of the key steps to determining the success in bone regeneration and ALP is one of the widely recognized markers of osteogenic differentiation, which regulates phosphate metabolism [82]. Previous research showed that magnesium and silicon ion release during the degradation of silicate-based bioceramics, e.g., bredigite, played an important role in raising ALP expression in BMSCs by providing a favorable ionic situation

[24] and recent studies have demonstrated that silicon or magnesium ions alone at a certain concentration enhance the ALP expression of BMSCs [83]. In our study, it was difficult to make an assertive conclusion as to whether it was one kind of ions alone or their combination that was responsible for the enhanced ALP expression of the Mg-40% bredigite composite, as compared with that of the monolithic magnesium. Nevertheless, it was clear from our results that the presence of silicon ions in the Mg-40% bredigite composite, with even a minor portion in the extract, contributed to a significantly enhanced ability to induce osteogenic differentiation and thus to an improved rate, quality and progression of bone healing, as has been demonstrated in the *in vivo* studies on Si-substituted materials [84].

Conclusions

1. Magnesium-matrix composites containing up to 40 vol.% bredigite particles and possessing strengths in the strength range of cortical bone could be successfully produced by using the PAS technique.
2. The addition of bredigite to magnesium could significantly slow down the biodegradation rate of magnesium by up to 24 times, due to the blocking effect of bredigite particles in the pitting pathways of the magnesium matrix and the embedding of slowly degrading bredigite in a surface layer of Mg, Ca, P and Si-containing compounds.
3. The mechanical functionality of magnesium could be extended from 3 days to more than 12 days. The strengths of the composites could be retained at a strength level of cortical bone after 12 days of immersion.
4. Bredigite-containing magnesium-matrix composites could improve the viability and proliferation of rat bone marrow stromal cells, while monolithic magnesium extracts without dilution were cytotoxic.
5. The magnesium-bredigite composites developed could have a great potential as a new generation of biodegradable and bioactive materials for orthopedic applications. The

achieved simultaneous improvements in degradation behavior, mechanical properties, biocompatibility and bioactivity prompted further *in vitro* and *in vivo* investigations.

Acknowledgements

This work was supported by the Netherlands Organization for Health Research and Development (ZonMw) under the project 1163500004 and the Chinese Academy of Sciences (CAS) under the External Cooperation Program, Grant no. GJHZ1211. Financial support from the National Natural Science Foundation of China (Grant No.: 81401529) and the One-Hundred Talent Program of SIC-CAS (Grant No.: Y36ZB1110G) is also gratefully acknowledged.

References

[1] M.E. Maguire, J.A. Cowan, Magnesium chemistry and biochemistry, BioMetals 15 (2002) 203-210.
[2] J. Marier, Dietary magnesium and drinking water: effects on human health status, Met. Ions Biol. Syst. 26 (1990) 85-104.
[3] C. Wen, Y. Yamada, K. Shimojima, Y. Chino, H. Hosokawa, M. Mabuchi, Compressibility of porous magnesium foam: dependency on porosity and pore size, Mater. Lett. 58 (2004) 357-360.
[4] F. Witte, J. Reifenrath, P. Müller, H.A. Crostack, J. Nellesen, F. Bach, et al., Cartilage repair on magnesium scaffolds used as a subchondral bone replacement, Materialwiss. Werkstofftech. 37 (2006) 504-508.
[5] L. Xu, G. Yu, E. Zhang, F. Pan, K. Yang, In vivo corrosion behavior of Mg- Mn- Zn alloy for bone implant application, J. Biomed. Mater. Res. A 83 (2007) 703-711.
[6] S. Naddaf Dezfuli, Z. Huan, J.M.C. Mol, M.A. Leeflang, J. Chang, J. Zhou, Influence of HEPES buffer on the local pH and formation of surface layer during in vitro degradation tests of magnesium in DMEM, Prog. Nat. Sci. 24 (2014) 531-538.
[7] N.T. Kirkland, J. Lespagnol, N. Birbilis, M.P. Staiger, A survey of bio-corrosion rates of magnesium alloys, Corros. Sci. 52 (2010) 287-291.

[8] A. Atrens, M. Liu, N.I. Zainal Abidin, Corrosion mechanism applicable to biodegradable magnesium implants, Mater. Sci. Eng. B 176 (2011) 1609-1636.
[9] S.S.A. El-Rahman, Neuropathology of aluminum toxicity in rats (glutamate and GABA impairment), Pharmacol. Res. 47 (2003) 189-194.
[10] S. Fenwick, E.A. Roberts, B.S. Mahesh, N.B. Roberts, In end-stage renal failure, does infection lead to elevated plasma aluminium and neurotoxicity? Implications for monitoring, Ann. Clin. Biochem. 42 (2005) 149-152.
[11] G. Song, Control of biodegradation of biocompatable magnesium alloys, Corros. Sci. 49 (2007) 1696-1701.
[12] N. Nassif, I. Ghayad, Corrosion protection and surface treatment of magnesium alloys used for orthopedic applications, Adv. Mater. Sci 2013 (2013) 1 – 10 (Article ID 532896).
[13] M.P. Staiger, A.M. Pietak, J. Huadmai, G. Dias, Magnesium and its alloys as orthopedic biomaterials: A review, Biomaterials 27 (2006) 1728-1734.
[14] X. Gu, W. Zhou, Y. Zheng, L. Dong, Y. Xi, D. Chai, Microstructure, mechanical property, bio-corrosion and cytotoxicity evaluations of Mg/HA composites, Mater. Sci. Eng. C 30 (2010) 827-832.
[15] F. Witte, F. Feyerabend, P. Maier, J. Fischer, M. Stormer, C. Blawert, et al., Biodegradable magnesium-hydroxyapatite metal matrix composites, Biomaterials 28 (2007) 2163-2174.
[16] D. Liu, Y. Zuo, W. Meng, M. Chen, Z. Fan, Fabrication of biodegradable nano-sized β-TCP/Mg composite by a novel melt shearing technology, Mater. Sci. Eng. C 32 (2012) 1253-1258.
[17] Y. Wang, Z.-h. Wu, H. Zhou, Z.-d. Liao, H.-f. Zhang, Corrosion properties in a simulated body fluid of Mg/β-TCP composites prepared by powder metallurgy, Int. J. Min. Met. Mater. 19 (2012) 1040-1044.
[18] M. Mastrogiacomo, A. Muraglia, V. Komlev, F. Peyrin, F. Rustichelli, A. Crovace, et al., Tissue engineering of bone: search for a better scaffold, Orthod. Craniofac. Res. 8 (2005) 277-284.
[19] E.M. Carlisle, Silicon: a possible factor in bone calcification, Science 167 (1970) 279-280.
[20] M. Vallet-Regí, D. Arcos, Silicon substituted hydroxyapatites. A method to upgrade calcium phosphate based implants, J. Mater. Chem. 15 (2005) 1509-1516.
[21] I. Gibson, S. Best, W. Bonfield, Chemical characterization of silicon- substituted hydroxyapatite, J. Biomed. Mater. Res. 44 (1999) 422-428.

[22] D. Yi, C. Wu, B. Ma, H. Ji, X. Zheng, J. Chang, Bioactive bredigite coating with improved bonding strength, rapid apatite mineralization and excellent cytocompatibility, J. Biomater. Appl. 28 (2014) 1343-1353.
[23] C. Wu, J. Chang, Synthesis and in vitro bioactivity of bredigite powders, J. Biomater. Appl. 21 (2007) 251-263.
[24] W. Zhai, H. Lu, C. Wu, L. Chen, X. Lin, K. Naoki, et al., Stimulatory effects of the ionic products from Ca–Mg–Si bioceramics on both osteogenesis and angiogenesis in vitro, Acta Biomater. 9 (2013) 8004-8014.
[25] C. Wu, J. Chang, J. Wang, S. Ni, W. Zhai, Preparation and characteristics of a calcium magnesium silicate (bredigite) bioactive ceramic, Biomaterials 26 (2005) 2925-2931.
[26] Z. Huang, S. Yu, Microstructure characterization on the formation of in situ Mg_2Si and MgO reinforcements in AZ91D/Flyash composites, J. Alloys Compd. 509 (2011) 311-315.
[27] Z. Huan, S. Leeflang, J. Zhou, W. Zhai, J. Chang, J. Duszczyk, In vitro degradation behavior and bioactivity of magnesium-Bioglass((R)) composites for orthopedic applications, J. Biomed. Mater. Res. B. Appl. Biomater. 100B (2011) 437-446.
[28] L. Xia, K. Lin, X. Jiang, Y. Xu, M. Zhang, J. Chang, Z. Zhang, Enhanced osteogenesis through nano-structured surface design of macroporous hydroxyapatite bioceramic scaffolds via activation of ERK and p38 MAPK signaling pathways, J. Mater. Chem. B 1 (2013) 5403-5416.
[29] J.R. Mauney, C. Jaquiéry, V. Volloch, M. Heberer, I. Martin, D.L. Kaplan, In vitro and in vivo evaluation of differentially demineralized cancellous bone scaffolds combined with human bone marrow stromal cells for tissue engineering, Biomaterials 26 (2005) 3173-3185.
[30] A.H. Cory, T.C. Owen, J.A. Barltrop, J.G. Cory, Use of an aqueous soluble tetrazolium/formazan assay for cell growth assays in culture, Cancer Commun. 3 (1991) 207-212.
[31] O.H. Lowry, N.R. Roberts, M.-L. Wu, W.S. Hixon, E.J. Crawford, The quantitative histochemistry of brain II. Enzyme measurements, J. Biol. Chem. 207 (1954) 19-38.
[32] B. Han, D. Dunand, Microstructure and mechanical properties of magnesium containing high volume fractions of yttria dispersoids, Mater. Sci. Eng. A 277 (2000) 297-304.
[33] M.M. Avedesian, H. Baker, ASM Specialty Handbook: Magnesium and Magnesium Alloys, ASM International, Ohio, 1999.
[34] E.F. Emley, Principles of Magnesium Technology, first ed., Pergamon Press, New York, 1966.
[35] T.H. Courtney, Mechanical Behavior of Materials, second ed., Waveland Press, Long Grove, 2005.

[36] R.d. Campo, B. Savoini, A. Muñoz, M.A. Monge, G. Garcés, Mechanical properties and corrosion behavior of Mg-HAP composites, J. Mech. Behav. Biomed. Mater. 39 (2014) 238-246.
[37] Y.F. Zheng, X.N. Gu, Y.L. Xi, D.L. Chai, In vitro degradation and cytotoxicity of Mg/Ca composites produced by powder metallurgy, Acta Biomater. 6 (2010) 1783-1791.
[38] A. Mazahery, M.O. Shabani, Plasticity and microstructure of A356 matrix nano composites, J. King Sad. Univ. Sci. 25 (2013) 41-48.
[39] S.R. Agnew, Ö. Duygulu, Plastic anisotropy and the role of non-basal slip in magnesium alloy AZ31B, Int. J. Plast. 21 (2005) 1161-1193.
[40] W.L. E Wong, M. Gupta, Simultaneously improving strength and ductility of magnesium using nano-size SiC particulates and microwaves, Adv. Eng. Mater. 8 (2006) 735-740.
[41] W.L.E. Wong, M. Gupta, Improving overall mechanical performance of magnesium using nano- alumina reinforcement and energy efficient microwave assisted processing route, Adv. Eng. Mater. 9 (2007) 902-909.
[42] I. Chang, Y. Zhao, Advances in Powder Metallurgy: Properties, Processing and Applications, Elsevier, London, 2013.
[43] S. Krishnamurthy, I. Weiss, F. Froes, Consolidation of rapidly solidified magnesium alloy powder, Key. Eng. Mater. 29 (1991) 135-146.
[44] A. Munitz, I.G. Jo, J. Nuechterlein, W. Garrett, J. Moore, M. Kaufman, Microstructural characterization of cast Mg-TiC MMC's, Int. J. Mater. Sci. 2 (2012) 15-19.
[45] K.S. Tun, W.L.E. Wong, Q.B. Nguyen, M. Gupta, Tensile and compressive responses of ceramic and metallic nanoparticle reinforced Mg composites, Materials 6 (2013) 1826-1839.
[46] L.L. Hench, Bioceramics: from concept to clinic, J. Am. Ceram. Soc. 74 (1991) 1487-1510.
[47] L.L. Hench, J. Wilson, An Introduction to Bioceramics, World Scientific, London, 1993.
[48] K.S. Katti, Biomaterials in total joint replacement, Colloids Surf. B Biointerfaces 39 (2004) 133-142.
[49] C. Taltavull, Z. Shi, B. Torres, J. Rams, A. Atrens, Influence of the chloride ion concentration on the corrosion of high-purity Mg, ZE41 and AZ91 in buffered Hank's solution, J. Mater. Sci. Mater. Med. 25 (2014) 329-345.
[50] R. Willumeit, J. Fischer, F. Feyerabend, N. Hort, U. Bismayer, S. Heidrich, et al., Chemical surface alteration of biodegradable magnesium exposed to corrosion media, Acta. Biomater. 7 (2011) 2704-2715.
[51] T. Lei, W. Tang, S.-H. Cai, F.-F. Feng, N.-F. Li, On the corrosion behaviour of newly developed biodegradable Mg-based metal matrix composites produced by in situ reaction, Corros. Sci. 54 (2012) 270-277.

[52] A. Yamamoto, S. Hiromoto, Effect of inorganic salts, amino acids and proteins on the degradation of pure magnesium in vitro, Mater. Sci. Eng. C 29 (2009) 1559-1568.
[53] G. Williams, H.N. McMurray, Localized corrosion of magnesium in chloride-containing electrolyte studied by a scanning vibrating electrode technique, J. Electrochem. Soc. 155 (2008) C340-C349.
[54] G. Williams, H. ap Llwyd Dafydd, R. Grace, The localised corrosion of Mg alloy AZ31 in chloride containing electrolyte studied by a scanning vibrating electrode technique, Electrochim. Acta 109 (2013) 489-501.
[55] M. Andrei, A. Eliezer, P.L. Bonora, E.M. Gutman, DC and AC polarization study on magnesium alloys Influence of the mechanical deformation, Mater. Corros. 53 (2002) 455-461.
[56] Y. Song, D. Shan, R. Chen, F. Zhang, E.-H. Han, Biodegradable behaviors of AZ31 magnesium alloy in simulated body fluid, Mater. Sci. Eng. C 29 (2009) 1039-1045.
[57] H. Liu, The effects of surface and biomolecules on magnesium degradation and mesenchymal stem cell adhesion, J. Biomed. Mater.Res. A 99A (2011) 249-260.
[58] Y. Yun, Z. Dong, D. Yang, M.J. Schulz, V.N. Shanov, S. Yarmolenko, et al., Biodegradable Mg corrosion and osteoblast cell culture studies, Mater. Sci. Eng. C 29 (2009) 1814-1821.
[59] G.-L. Song, Corrosion of Magnesium Alloys, Woodhead Publishing, Oxford, 2011.
[60] L. Yang, X. Zhou, S.-M. Liang, R. Schmid-Fetzer, Z. Fan, G. Scamans, et al., Effect of traces of silicon on the formation of Fe-rich particles in pure magnesium and the corrosion susceptibility of magnesium, J. Alloys. Compd. 619 (2015) 396-400.
[61] G.L. Song, A. Atrens, Corrosion Mechanisms of Magnesium Alloys, Adv. Eng. Mater. 1 (1999) 11 - 33.
[62] S. Bender, J. Goellner, A. Heyn, S. Schmigalla, A new theory for the negative difference effect in magnesium corrosion, Mater. Corros. 63 (2012) 707-712.
[63] J. Jia, H. Zhou, J. Wei, X. Jiang, H. Hua, F. Chen, et al., Development of magnesium calcium phosphate biocement for bone regeneration, J. R. Soc. Interface 7 (2010) 1171-1180.
[64] M. Razavi, M. Fathi, O. Savabi, S. Mohammad Razavi, B. Hashemi Beni, D. Vashaee, et al., Controlling the degradation rate of bioactive magnesium implants by electrophoretic deposition of akermanite coating, Ceram. Int. 40 (2014) 3865-3872.
[65] X. Liu, C. Ding, P.K. Chu, Mechanism of apatite formation on wollastonite coatings in simulated body fluids, Biomaterials 25 (2004) 1755-1761.
[66] P.A.A.P. Marques, A.P. Serro, B.J. Saramago, A.C. Fernandes, M.C.F. Magalhaes, R.N. Correia, Mineralisation of two calcium phosphate ceramics in biological model fluids, J. Mater. Chem. 13 (2003) 1484-1490.

[67] J. Faix, D. Breitsprecher, T. E. B. Stradal, K. Rottner, Filopodia: Complex models for simple rods, Inter. J. Biochem. Cell Biol. 41 (2009) 1656-1664.
[68] S.V. Dorozhkin, Calcium orthophosphate coatings on magnesium and its biodegradable alloys, Acta Biomater. 10 (2014) 2919-2934.
[69] J. Waterman, A. Pietak, N. Birbilis, T. Woodfield, G. Dias, M.P. Staiger, Corrosion resistance of biomimetic calcium phosphate coatings on magnesium due to varying pretreatment time, Mater. Sci. Eng. B 176 (2011) 1756-1760.
[70] Z.L. Sun, J.C. Wataha, C.T. Hanks, Effects of metal ions on osteoblast-like cell metabolism and differentiation, J. Biomed. Mater. Res. 34 (1997) 29-37.
[71] H.-S. Han, Y. Minghui, H.-K. Seok, J.-Y. Byun, P.-R. Cha, S.-J. Yang, et al., The modification of microstructure to improve the biodegradation and mechanical properties of a biodegradable Mg alloy, J. Mech. Behav. Biomed. Mater. 20 (2013) 54-60.
[72] X. Gu, Y. Zheng, Y. Cheng, S. Zhong, T. Xi, In vitro corrosion and biocompatibility of binary magnesium alloys, Biomaterials 30 (2009) 484-498.
[73] C.-h. Ye, T.-f. Xi, Y.-f. Zheng, S.-q. Wang, L. Yang-de, In vitro corrosion and biocompatibility of phosphating modified WE43 magnesium alloy, Trans. Nonferrous Met. Soc. China 23 (2013) 996-1001.
[74] L. Yang, N. Hort, D. Laipple, D. Höche, Y. Huang, K.U. Kainer, et al., Element distribution in the corrosion layer and cytotoxicity of alloy Mg–10Dy during in vitro biodegradation, Acta Biomater. 9 (2013) 8475-8487.
[75] X. Gu, N. Li, Y. Zheng, L. Ruan, In vitro degradation performance and biological response of a Mg–Zn–Zr alloy, Mater. Sci. Eng. B 176 (2011) 1778-1784.
[76] B. Zhang, Y. Hou, X. Wang, Y. Wang, L. Geng, Mechanical properties, degradation performance and cytotoxicity of Mg–Zn–Ca biomedical alloys with different compositions, Mater. Sci. Eng. C 31 (2011) 1667-1673.
[77] H. Li, Q. Peng, X. Li, K. Li, Z. Han, D. Fang, Microstructures, mechanical and cytocompatibility of degradable Mg–Zn based orthopedic biomaterials, Mater. Des. 58 (2014) 43-51.
[78] Y. Sun, B. Zhang, Y. Wang, L. Geng, X. Jiao, Preparation and characterization of a new biomedical Mg–Zn–Ca alloy, Mater. Des. 34 (2012) 58-64.
[79] M. Gupta, G.K. Meenashisundaram, Insight into Designing Biocompatible Magnesium Alloys and Composites: Processing, Mechanical and Corrosion Characteristics, Springer, New York, 2015.

[80] H. Sun, C. Wu, K. Dai, J. Chang, T. Tang, Proliferation and osteoblastic differentiation of human bone marrow-derived stromal cells on akermanite-bioactive ceramics, Biomaterials 27 (2006) 5651-5657.
[81] L. Tan, X. Yu, P. Wan, K. Yang, Biodegradable materials for bone repairs: a review, J. Mater. Sci. Technol. 29 (2013) 503-513.
[82] R. Marom, I. Shur, R. Solomon, D. Benayahu, Characterization of adhesion and differentiation markers of osteogenic marrow stromal cells, J. Cell Physiol. 202 (2005) 41-48.
[83] P. Han, C. Wu, Y. Xiao, The effect of silicate ions on proliferation, osteogenic differentiation and cell signaling pathways (WNT and SHH) of bone marrow stromal cells, Biomater. Sci. 1 (2013) 379-392.
[84] K.A. Hing, P.A. Revell, N. Smith, T. Buckland, Effect of silicon level on rate, quality and progression of bone healing within silicate-substituted porous hydroxyapatite scaffolds, Biomaterials 27 (2006) 5014-5026.